Maritime Technology and Research

https://so04.tci-thaijo.org/index.php/MTR

Research Article

Effects of a long-drive shaft on flow field around a high-speed boat propeller in Thailand using CFD

Prachakon Kaewkhiaw*

Department of Maritime Engineering, Faculty of International Maritime Studies, Kasetsart University, Sriracha Campus, Sri Racha, Chonburi 20230, Thailand

Article information

Received: November 29, 2023
1st Revision: January 18, 2024
2nd Revision: February 11, 2024
Accepted: February 16, 2024

Keywords
Long-Drive Shaft (LDS),
Long-Tail Boat (LTB),
Inclined Shaft Propeller,
Reynolds Averaged Navier-Stokes (RANS),
Computational Fluid Dynamics (CFD)

Abstract

The Long-Tail Boat (LTB) is a high-speed boat in Thailand. The propulsive system has a long-drive shaft that holds the propeller on the end of the shaft. It is used under inclined shaft conditions because of shallow water draft. Thus, the fluid flow into the propeller blade area is unsteady due to the cross-flow component. Therefore, the long-drive shaft is an important parameter in generating the flow field before entering the propeller blades, which affects propeller efficiency. This paper presents a numerical analysis of the flow field around a long-drive shaft and propeller blade areas in a full-scale propeller size using the Reynolds-Averaged Navier-Stokes (RANS) solver. The unsteady propeller performance is carried out by considering inclined flow conditions. In addition, the computational results of fluid flow in terms of the pressure distributions and wake fields around a long-drive shaft and propeller are investigated, which influence the propeller performance and the generating drag forces by a long-drive shaft. The results can be applied to modify the long-drive shaft of boats.

1. Introduction

The Long-Tail Boat (LTB) is a local vessel in Thailand that has a high speed. It was established by the Thai people in 1,932. It is classified as a type of planing hull due to the draft water being shallow. The hull has length, breadth, depth, and draft of 8.88, 1.60, 0.72, and 0.27 m, respectively. The hull is divided into two-step hulls to reduce wetted surface areas. Therefore, it is often applied to high-speed passenger vessels on rivers, with a maximum speed equal to approximately 37 knots, and an operating speed of about 27 knots. The LBT can hold about 8 passengers. The propulsion system consists of an engine installed on a boat stern. The long-drive shaft is connected to the engine, which can rotate in a semicircle to control the boat's direction without using the rudder. The propeller is mounted directly to the end of the long-drive shaft, which is covered with a hollow metal rod without a gearbox. **Figure 1** shows the Long-Tail Boat which has been studied in this research.

*Corresponding author: *Department of Maritime Engineering, Faculty of International Maritime Studies, Kasetsart University, Sriracha Campus, Sri Racha, Chonburi 20230, Thailand*
E-mail address: prachakon.ka@ku.th

Figure 1 Hull and propulsion system of the Long-Tail Boat.

Experiments on inclined shaft conditions interest many researchers because they can be applied to conduct experiments on high-speed vessels, such as the investigations into propeller cavitation in oblique flow conditions performed at the Mitsubishi experimental tank by Taniguchi et al. (1969). Peck and Moore (1974) evaluated the forces generated by inclined-shaft propellers for the design of high-performance small craft. Alder and Moore (1977) measured the effect of shaft inclination from the horizontal in partially submerged operations to different shaft yaw angles on propeller performance for a highly skewed propeller. Recently, Aktas et al. (2015) investigated the shaft inclination on propeller efficiency, cavitation, and underwater radiated noise characteristics in a cavitation tunnel. Ortolani and Dubbioso (2019) described the measurement of a single blade and propeller loads by a free-running model test for a straight ahead sailing and steady ship motion case. This was studied to investigate the hydrodynamic interactions between the hull's wake and the propeller, which is operated inclining. The propeller performance on straight and steady drift motions for single blade loads, including the flow field measurement using Stereoscopic Particle Image Velocimetry (SPIV) (SPIV) with the ship model, has been analyzed by Ortolani et al. (2020). Efremov (2021) studied the effectiveness of a ship's twin propeller system in maneuvering by taking into account the influence of the oblique flow to the "internal" and "external" propellers respective to the trajectory of motion. The effect of immersion depth on semi-submersible surface-piercing propellers in a towing tank was assessed by Seyyedi et al. (2022). Abbasi et al. (2023) presented an experimental analysis of the velocimetric measurements, the flow field generated by a marine propeller running with an inclined shaft, by using Laser Doppler Velocimetry (LDV) in a cavitation tunnel.

Meanwhile, computational fluid dynamics (CFD) have been studied to investigate propeller performance with inclined shaft propellers, Yao (2015) presented a numerical study investigating hydrodynamic characteristics of a marine propeller in oblique flow, achieved by RANS simulations. Numerical analysis of unsteady hydrodynamic performance in oblique flow by using CFD commercial software code FLUENT was considered by Wang et al. (2017). Gaggero and Villa (2018) proposed cavitating propeller performance with inclined shaft conditions with OpenFOAM (PPTC 2015 Test Case). Paik et al. (2020) studied open water propeller performance with sinusoidal pitch motion, which was set at inclined angles (–10° to 10°) by STAR-CCM+ software. An optimization procedure for propeller selection for different shaft inclinations has been conducted by Soares et al. (2022). Zheng et al. (2022) offered a numerical investigation of propeller cavitation benchmark tests in oblique flow based on OpenFOAM software. The literature reviews did not find any previous research on long-drive shaft propellers, because they are only used

for Long-Tail Boats, which is a local boat in Thailand. However, it was found that Kaewkhiaw (2018, 2020) studied the steady and unsteady propeller performance operating at different yaw angles and the inclined shaft angle conditions for the Long-Tail Boat. It was intended to investigate the suitability of working conditions of the Long-Tail Boat. Additionally, the integrative for the Long-Tail Boat propeller and the propeller boss cap fins (PBCF) with inclination as per real life was analyzed, in order to increase performance, using the Reynolds-averaged Navier-Stokes (RANS) by Kaewkhiaw (2021).

This paper proposes computational fluid dynamics (CFD) code ANSYS Fluent to study the effect of a long-drive shaft propeller on the phenomenon of fluid flow around it, and the propeller, of the Long-Tail Boat. The drag force from a long-drive shaft affects the total propeller performance. The numerical results show an unsteady performance from the inclined shaft condition. The pressure distributions and wake fields around a long-drive shaft and propeller are investigated to ascertain the propeller thrust and drag forces by the long-drive shaft, including propeller efficiency.

2. Long-drive shaft and propeller of Long-Tail Boat

A long-drive shaft is covered by a hollow metal rod which is set at an inclined angle approximately 12° from the horizontal axis. The length of the long-drive shaft is 4.5 m, and the diameter of the metal rod is about 6 cm, as shown in **Figure 2**. The propeller diameter is 34 cm, which is installed directly on the end of a long-drive shaft without a gearbox. For this reason, it may be concluded that Long-Tail Boats are a special type of high-speed vessel because the drive shaft is long, unlike other general high-speed boats.

The computational calculation for the effect of a long-drive shaft on the flow field around the propeller is performed in full-scale propeller size, which is the same as the actual boat. **Figure 3** shows a long-drive shaft propeller in a numerical simulation. The characteristics of an actual long-drive shaft and propeller are presented in **Table 1**. The other details of the Long-Tail Boat propeller can be found in Kaewkhiaw (2021).

Figure 2 Photograph of the long-drive shaft and propeller for the Long-Tail Boat.

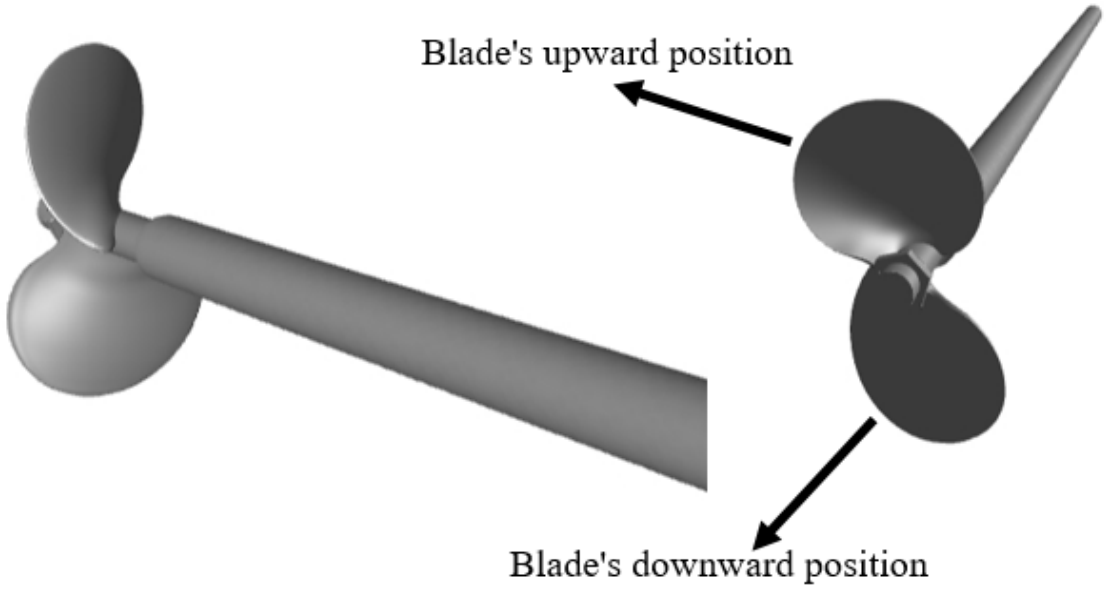

Figure 3 Long-drive shaft and propeller in full-scale propeller size for computation.

Table 1 Actual principal particulars of long-drive shaft and propeller for the Long-Tail Boat.

Number of blades	2
Hub diameter ratio	0.14
Expanded area ratio	0.6
Direction of rotation	Right hand
Propeller diameter (m)	0.34
Design advance coefficient (J)	1.1
Inclined shaft angle (degrees)	12
Long-drive shaft (m)	4.5
Long-drive shaft diameter (cm)	6

Components of the inflow and generating forces of the propeller, as well as the drag forces due to the effect of a long-drive shaft for the propeller with operating inclined shaft angles, are demonstrated in **Figure 4**. Inflow velocity, V_{in}, is divided into two components on the long-drive shaft plane. The first, $V_{in} \cos\theta$, is in the long-drive shaft axial direction, and the second, $V_{in} \sin\theta$, is in the vertical direction of the long-drive shaft, where θ is the angle of the inclined shaft angle to the horizontal axis. At the same time, the propeller will generate the axial thrust, T, which can be separated into two components. The first, $T \cos\theta$, is the propeller thrust force to push the hull forward along the horizontal axis. The second, $T \sin\theta$, is the propeller thrust force in the vertical, which causes the stern rise. Moreover, a long-drive shaft generates forces (drag force) opposite the propeller's thrust, which raises the resistance of the Long-Tail Boat at each speed range. Therefore, the total propeller thrust to push the hull forward along the horizontal axis is reduced.

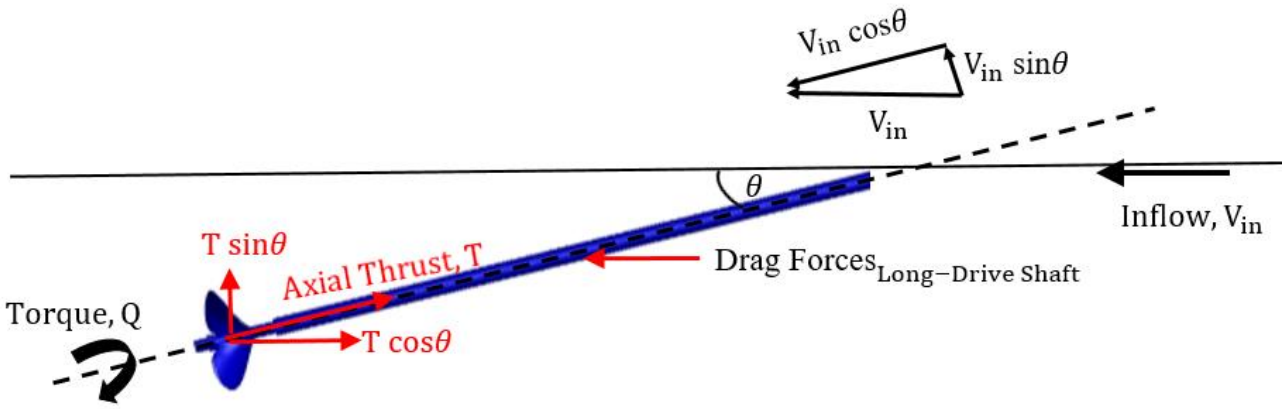

Figure 4 Diagram of inflow velocity, propeller forces, and drag forces with a long-drive shaft for the Long-Tail Boat.

3. Numerical method

The governing equations can be derived by the conservation of mass and momentum equations. These have been applied in their incompressible form and the general Reynolds Averaged Navier-Stokes (RANS) equations. The conservation of mass or continuity equation can be written as follows (ANSYS Fluent Theory Guide, 2021):

$$\frac{\partial \rho}{\partial t} + \nabla \cdot (\rho \vec{v}) = S_m \tag{1}$$

The source, S_m, is the mass added to the continuous phase from the dispersed second phase (for example, due to the vaporization of liquid droplets) and any user-defined sources.

The conservation of momentum equations is as follows (ANSYS Fluent Theory Guide, 2021):

$$\frac{\partial}{\partial t}(\rho \vec{v}) + \nabla \cdot (\rho \vec{v}\vec{v}) = -\nabla p + \nabla \cdot (\bar{\bar{\tau}}) + \rho \vec{g} + \vec{F} \tag{2}$$

Where p is the static pressure, $\bar{\bar{\tau}}$ is the stress tensor, and $\rho \vec{g}$ and $\vec{F}$ are the gravitational body force and external body forces, respectively. $\vec{F}$ contains other model-dependent source terms such as porous media and user-defined sources.

The stress tensor $\bar{\bar{\tau}}$ is given by

$$\bar{\bar{\tau}} = \mu \left[(\nabla \vec{v} + \nabla \vec{v}^T) - \frac{2}{3} \nabla \cdot \vec{v} I \right] \tag{3}$$

Where μ is the molecular viscosity, I is the unit tensor, and the second term is on the right hand side which has the effect of volume dilation.

The SST k-ω model was applied in this study. This has been employed to calculate the Reynolds-Stress term in the RANS equations. The SST k-ω equations are written as follows (ANSYS Fluent Theory Guide, 2021):

$$\frac{\partial}{\partial t}(\rho k) + \frac{\partial}{\partial x_i}(\rho k u_i) = \frac{\partial}{\partial x_j}\left(\Gamma_k \frac{\partial k}{\partial x_j} \right) + G_k - Y_k + S_k + G_b \tag{4}$$

$$\frac{\partial}{\partial t}(\rho \omega) + \frac{\partial}{\partial x_j}(\rho \omega u_j) = \frac{\partial}{\partial x_j}\left(\Gamma_\omega \frac{\partial \omega}{\partial x_j} \right) + G_\omega - Y_\omega + S_\omega + G_{\omega b} \tag{5}$$

In these equations, G_k represents the generation of turbulence kinetic energy due to mean velocity gradients. G_ω represents the generation of ω. Γ_k and Γ_ω represent the effective diffusivity of k and ω, respectively. Y_k and Y_ω represent the dissipation of k and ω due to turbulence. S_k and S_ω are user-defined source terms. G_b and $G_{\omega b}$ account for buoyancy terms as described in terms of effects of buoyancy on turbulence in the k-ω models.

The governing equations are discretized by using the finite volume method. The pressure-velocity coupling is achieved through the SIMPLE algorithm. The Second Order Upwind scheme is imposed for the discretization of the momentum equation. The gradient discretization is solved by using Least Squares Based. Other details can be found in the ANSYS Fluent Theory Guide, 2021.

4. Computational domain and grid generation

The flow field around a long-drive shaft and the propeller areas with operating inclined shaft conditions is asymmetrical. The periodic boundary condition technique cannot be applied in this case. Therefore, the computational domain should be conducted as whole domains with oblique flow. The domains are divided into stationary and rotating regions. First, the fixed part is called the stationary region. Second, the fluid flows are rotated around the propeller areas which corresponds to the propeller revolution, and is called the rotating region by using the moving reference frame (MRF) techniques. This solves fluid cell zones in a steady state. The flow field represents a snapshot of the transient flow field in which the rotating parts move. Other details of MRF can be found in the ANSYS Fluent User's Guide, 2021.

The calculation domain with full-blade propellers operating inclined shaft conditions is illustrated in **Figure 5**. The inlet of inflow velocity, V_{in}, is decomposed into the shaft axial direction which is assigned to $V_x = V_{in} \cos\theta$, and the shaft vertical direction which is given to $V_Z = V_{in} \sin\theta$. The inclined shaft angle, θ is conducted at 12° from the horizontal axis in this study, which is consistent with the actual use of the Long-Tail Boat. The outlet imposes the pressure on the far-field. The turbulence intensity and turbulence viscosity ratio at the boundary inlet is defined as equal to 1 %. The dimensions of the mathematical domain are presented in **Table 2**, which has been studied by Kaewkhiaw (2020).

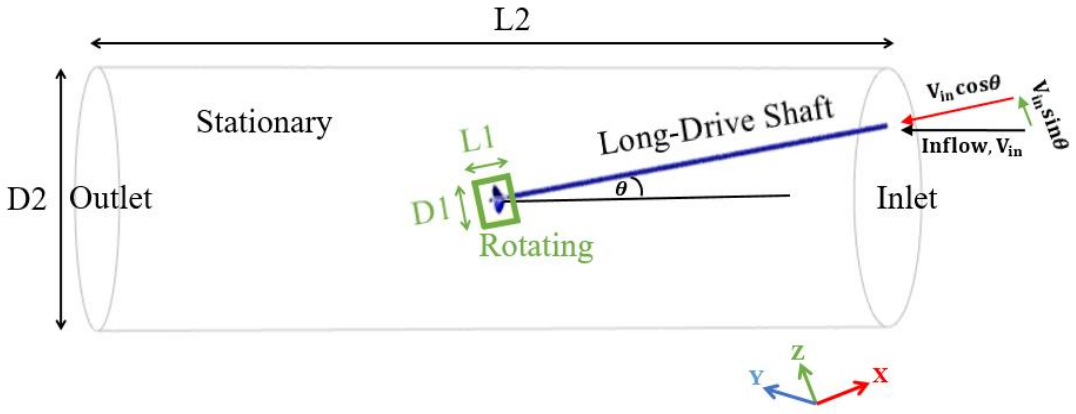

Figure 5 Computational domain of inclined shaft propeller with a long-drive shaft.

Table 2 Dimensions of computational domain for inclined shaft conditions with a long-drive shaft.

	Stationary	Rotating
D1		1.50D
D2	8.80D	
L1		1.20D
L2	27.10D	

The grid quality of computational domains with inclined shaft propellers in full-scale propeller size for Long-Tail Boats was investigated by Kaewkhiaw (2021). Therefore, this research is based on previous studies on grid quality. The grid independence was studied to ensure the accuracy of computational results in this research by separating them into three cases, which are presented in **Table 3**. The first one is called Grid 1, which is the coarse grid. Next, it is applied to the grid better than Grid 1, called Grid 2. Finally, it is modified to a finesse grid, called Grid 3. **Figure 6** presents the numerical grids in the calculation domains, and the surface grid on the propeller blades is shown in **Figure 7**. The computational domains of stationary and rotating regions are divided into discrete control volumes by the polyhedral grids, which are highly flexible and suitable for a long-drive shaft and propellers. The propeller and hub surfaces are determined by finesse grids and the boundary prism layers on near-blade surfaces to solve the viscous layer problem. The surrounding area of the blade surface creates a larger grid. The adaptive grid refinement techniques have been modified to them. The first layer thickness of the prism layer is determined by a non-dimensional wall distance on the surfaces of the propeller. The other layers are conducted to increase the rate of prism layer thickness. The average values of Y-plus on the location of the first grid point at a distance from the solid surfaces are defined as about 1. The surrounding area has been kept below 30 for the finesse grid, which corresponds to the ITTC recommended procedures and guidelines, section 7.5-03-02-03 (2011).

The numerical calculations are conducted on a personal computer with a 64-bit operating system, x64-based processor. AMD Ryzen 7, PRO 3700, 8-Core Proceesor@3.6 GHz, and 32 GB of RAM. The computation processing time of the parallel processor (16 CPUs) is approximately 6 hours per advance coefficient to achieve the convergence requirements of $1e^{-06}$.

Table 3 Grid specifications of the computational domain for inclined shaft condition with a long-drive shaft.

Grid configuration	Grid 1	Grid 2	Grid 3
	Coarse	Medium	Fine
Grid type	Polyhedral	Polyhedral	Polyhedral
Total	1.5 M	3 M	5 M
Rotating region	1 M	2 M	3 M
Stationary region	0.5 M	1 M	2 M

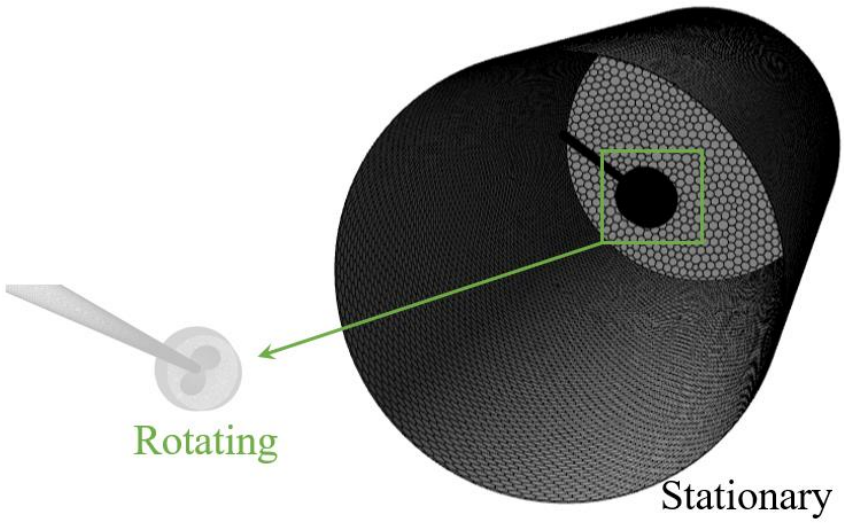

Figure 6 Grid of computational domains for rotating and stationary regions.

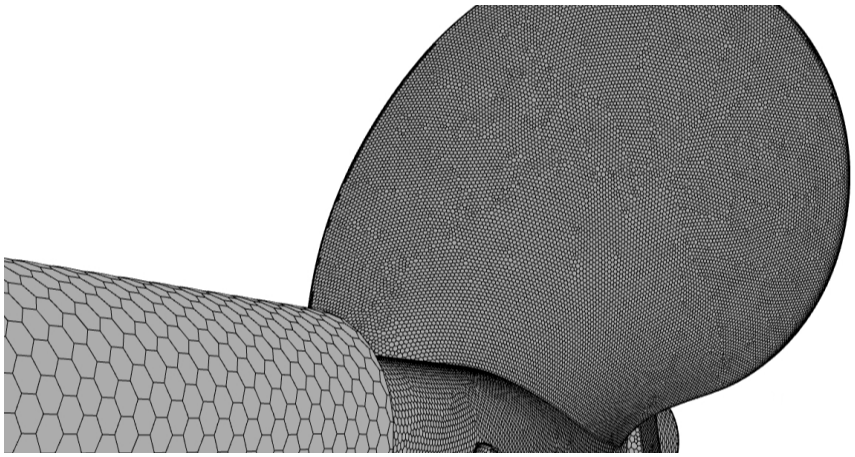

Figure 7 Polyhedral grids on the long-drive shaft propeller.

5. Results and discussion

The computational results of the propeller performance operating under the straight shaft condition (without inclined shaft angle), compared to each other in the model-scale propeller size, are shown in **Figure 8**. It was found that the thrust and torque coefficients, including propeller efficiency (blue dashed line), in this case were very good in each range of advanced coefficients [J] when compared to the measurement data (square point) of the open water test (without a long-drive shaft) at the high-speed circulating water channel at Kyushu University conducted by Kaewkhiaw et al. (2015).

Regarding the full-scale propeller size, the propeller performance of calculated results was compared with the experimental data to verify grid quality. It seems the propeller performance by Grid 3 (green solid line) is closest to the test data when compared to each other. Therefore, this paper focuses only on the results of Grid 3. It appears that the torque coefficient of Grid 3 (green solid line) was slightly increased from the model scale (blue dashed line) and experiment (square point) at the higher advance coefficients. This result may be due to the scale effect of the propeller size. However, the tendency of propeller efficiency of Grid 3 (green solid line) has a good relationship with the experimental data (square point). Unfortunately, the test for inclined shaft condition with a long-drive shaft was not measured because of the limitations of the experimental equipment.

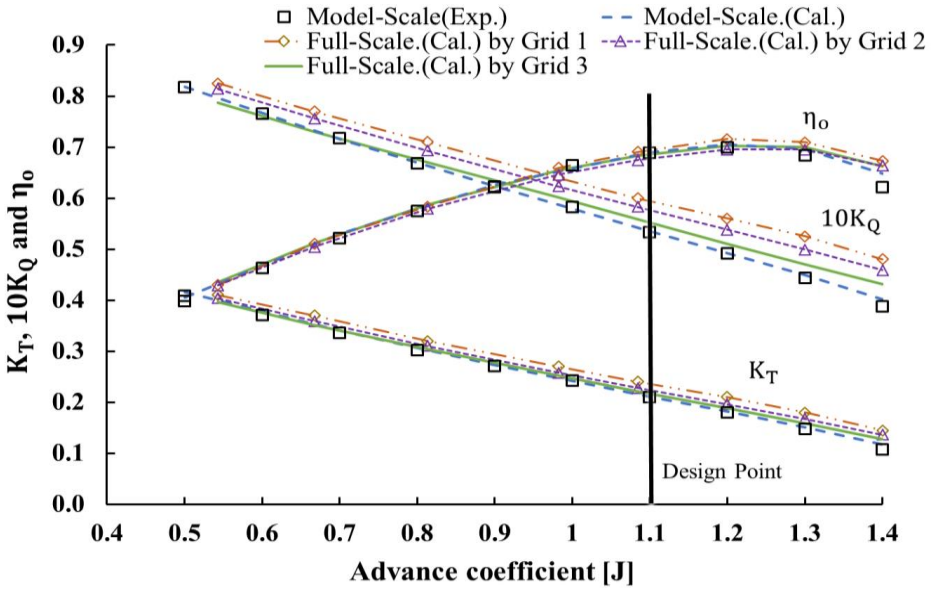

Figure 8 Comparison of propeller performance operating under straight shaft condition without a long-drive shaft.

The unsteady propeller performance operating under straight condition between without and with a long-drive shaft is presented in **Figure 9**. The thrust coefficient (red dashed line) with a long-drive shaft was slightly decreased compared to without a long-drive shaft (green solid line) at each range of advance coefficients [J]. The torque coefficient (red dashed line) with a long-drive shaft at advance coefficient J < 0.7 is similar to the value without a long-drive shaft. Maybe the long-drive shaft has a small effect at low speeds. However, the torque coefficient (red dashed line) with a long-drive shaft at J > 0.7 is decreased compared to without a long-drive shaft (green solid line). It can be seen that the value of propeller efficiency with a long-drive shaft (red dashed line) is lower than the value without a long-drive shaft (green solid line) at each range of advance coefficients [J].

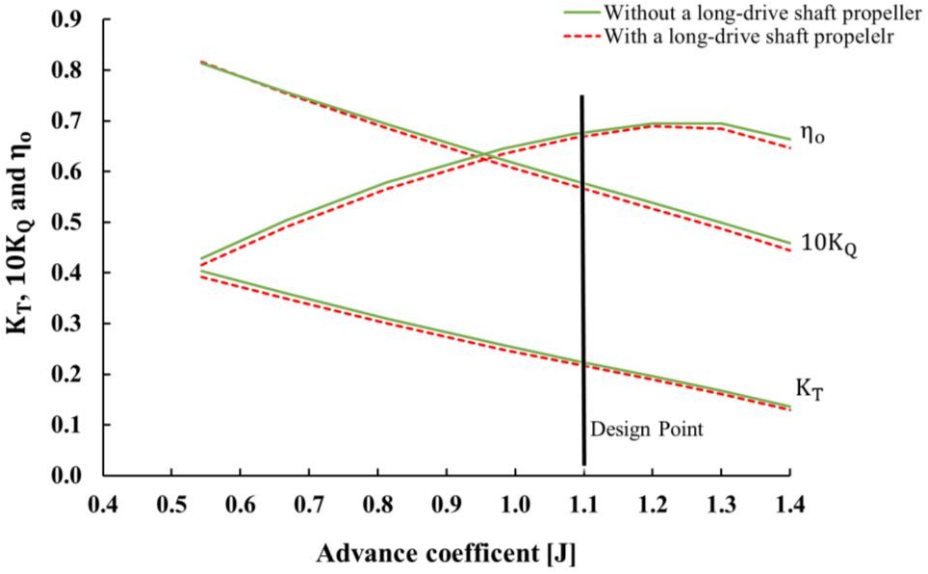

Figure 9 Comparison of propeller performance operating under straight shaft condition in full-scale propeller size between without and with a long-drive shaft.

Table 4 Propeller performance between without and with a long-drive shaft operating under straight shaft propeller condition.

Testing problems from the boat sea trials				Total Thrust (N)			Total Torque (N·m)			Propeller Efficiency		
J	N (rpm)	D (m)	Vin (m/s)	Without LDS	With LDS	% of decreasing	Without LDS	With LDS	% of decreasing	Without LDS	With LDS	% of decreasing
0.5	1,353.30	0.34	4.167	2,738.66	2,657.71	-2.96	187.56	188.26	0.37	0.43	0.42	-3.32
0.7	1,468.40	0.34	5.556	2,866.30	2,781.28	-2.97	205.20	204.69	-0.25	0.50	0.49	-2.72
0.8	1,567.20	0.34	7.222	2,821.28	2,730.58	-3.22	214.32	212.21	-0.98	0.58	0.57	-2.25
1.0	1,945.90	0.34	10.833	3,608.48	3,489.60	-3.29	297.02	292.31	-1.59	0.65	0.63	-1.74
1.1	2,305.30	0.34	14.167	4,483.98	4,343.05	-3.14	390.06	382.40	-1.96	0.67	0.67	-1.20
1.2	2,543.10	0.34	17.293	4,691.26	4,547.87	-3.06	438.10	428.44	-2.21	0.70	0.69	-0.87
1.3	2,761.00	0.34	20.339	4,732.62	4,546.38	-3.94	478.92	467.29	-2.43	0.70	0.68	-1.54
1.4	3,005.40	0.34	23.843	4,566.90	4,321.23	-5.38	521.70	505.89	-3.03	0.66	0.65	-2.42

Where LDS is long-drive shaft.

Table 4 shows the thrust, torque coefficients, and propeller efficiency between without and with a long-drive shaft (LDS). The boundary conditions in the computation were defined to be the same as the actual conditions of the Long-Tail Boat in sea trials in a river in Thailand. It is clearly found that the value of propeller performance in terms of the thrust, torque coefficients, and propeller efficiency with a long-drive shaft showed a decrease compared to without a long-drive shaft at each range of advance coefficients [J]. Therefore, the long-drive shaft obstructs fluid flow that enters the propeller, which generates the drag forces. Furthermore, decreasing percentages of total thrust decrease with the high velocity of the inflow. It was found that the total thrust is reduced by about 3.14 % at the design point.

The propeller performance, in terms of the average thrust, torque coefficients, and propeller efficiency, operating under the straight shaft angle and operating under the inclined angle of 12° with a long-drive shaft is demonstrated in **Figure 10**. It seemed the thrust and torque coefficients operating under the inclined shaft condition (black solid line) are lower than when operating without the inclined shaft condition (straight shaft condition) (red dashed line) at advance coefficient $J < 1.0$. However, the torque coefficient operating under inclined shaft angles (black solid line) showed an increase compared to operating without inclined shaft condition (red dashed line) at $J > 1.0$. The values of thrust coefficient are seen to be similar between operating without inclined shaft conditions (red dashed line) and operating with inclined shaft conditions (black solid line) at $J > 1.0$ or where there is a high velocity of inflow. However, propeller efficiency operating under an inclined shaft angle (black solid line) decreased compared to operating under the straight shaft condition (red dashed line) at each range of advance coefficients [J].

Table 5 presents the unsteady calculation results with a long-drive shaft operating under the straight shaft condition and operating under the inclined shaft condition. The boundary conditions in the computation were carried out to be the same as for the boat sea trials in the river. It was found that the percentage of decrease for the thrust and torque coefficients between operating inclined shaft angle versus operating straight shaft condition showed negative values at $J < 1.0$ or low inflow velocity. Meanwhile, the percentage of decrease for the thrust and torque coefficients between operating under inclined shaft angle versus operating under straight shaft condition showed positive values at $J > 1.0$, or high inflow velocity. It is clearly seen that the percentage of decrease for the propeller efficiency between operating under inclined shaft angle versus operating under straight shaft condition displayed negative values at each range of advance coefficients [J]. The higher advance coefficients, the percentage of decrease in the propeller efficiency operating under inclined shaft conditions versus operating under straight shaft conditions shows the severity. The propeller efficiency of the inclined shaft condition is reduced by about 3.21 % when compared to the operating under straight shaft condition at the design point.

One reason for those results is that the phenomenon of fluid flows with inclined shaft conditions is more complicated than with straight shaft conditions. In the inclined shaft condition, the velocity of fluid flows on each blade surface is different. Flow velocity between the blade's upward position and the blade’s downward position is different; therefore, the propeller generates the thrust and torque on each rotational angle with inconstancy. Additionally, the propeller characteristics, in terms of pitch distribution, skew, and rake angles, are not designed to operate under inclined shaft angles, and the propeller generates uneven thrust and torque, which causes the propeller efficiency to decrease.

The drag forces generated by a long-drive shaft operating under the straight shaft and inclined shaft conditions are illustrated in **Table 6**. It is found that the tendency of drag forces for operating an inclined angle increases with a high advance coefficient [J] or high velocity of inflow. However, the drag forces operating under straight shaft condition is very small in each range of advance coefficient, as well as at the design point.

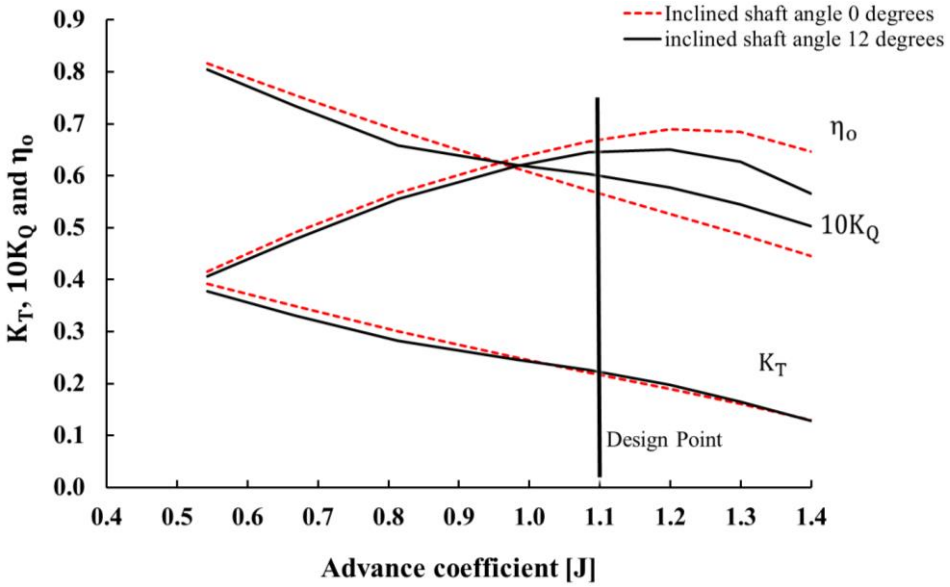

Figure 10 Comparison of propeller performance between operating under straight shaft and inclined shaft conditions in full-scale propeller size with a long-drive shaft propeller.

Table 5 Propeller performance with a long-drive shaft operating under straight shaft and inclined shaft conditions.

Testing problems from the boat sea trials				Total Thrust (N)			Total Torque (N·m)			Propeller Efficiency		
				Inclined shaft angles			Inclined shaft angles			Inclined shaft angles		
J	N (rpm)	D (m)	Vin (m/s)	0 (degrees)	12 (degrees)	% of decreasing	0 (degrees)	12 (degrees)	% of decreasing	0 (degrees)	12 (degrees)	% of decreasing
0.5	1,353.30	0.34	4.167	2,657.71	2,562.53	-3.58	188.26	185.53	-1.45	0.42	0.41	-2.16
0.7	1,468.40	0.34	5.556	2,781.28	2,634.72	-5.27	204.69	199.30	-2.63	0.49	0.48	-2.71
0.8	1,567.20	0.34	7.222	2,730.58	2,563.97	-6.10	212.21	203.32	-4.19	0.57	0.55	-1.99
1.0	1,945.90	0.34	10.833	3,489.60	3,441.95	-1.37	292.31	295.80	1.19	0.63	0.62	-2.53
1.1	2,305.30	0.34	14.167	4,343.05	4,438.89	2.21	382.40	403.79	5.59	0.67	0.65	-3.21
1.2	2,543.10	0.34	17.293	4,547.87	4,710.51	3.58	428.44	470.25	9.76	0.69	0.65	-5.63
1.3	2,761.00	0.34	20.339	4,546.38	4,651.04	2.30	467.29	522.32	11.78	0.68	0.63	-8.48
1.4	3,005.40	0.34	23.843	4,321.23	4,265.67	-1.29	505.89	571.55	12.98	0.65	0.57	-12.63

Figure 11 presents the computational results of pressure coefficient distributions on, chord-wise, blade positions r/R = 0.5, 0.7, and 0.9, respectively, at the design point operating under the straight shaft and inclined shaft conditions, corresponding to propeller performance in **Figure 10**. It is found that the pressure at the pressure side and suction side in x/C = 0.3 to 1.0 on all chord-wise blade positions operating under the inclined shaft angle (black solid line) was slightly increased than under the straight shaft condition (red dashed line).

Table 6 The drag forces of a long-drive shaft operating in the different conditions.

Testing problems from the boat sea trials				Drag forces for a long drive-shaft (N)	
				Inclined shaft angles (degrees)	
J	**N (rpm)**	**D (m)**	**Vin (m/s)**	**0 (degrees)**	**12 (degrees)**
0.5	1,353.30	0.34	4.167	0.13	21.67
0.7	1,468.40	0.34	5.556	0.18	38.81
0.8	1,567.20	0.34	7.222	0.23	60.98
1.0	1,945.90	0.34	10.833	0.39	148.33
1.1	2,305.30	0.34	14.167	0.59	253.62
1.2	2,543.10	0.34	17.293	0.78	378.01
1.3	2,761.00	0.34	20.339	0.99	523.36

The computation contours of average pressure coefficient distribution on the pressure side and suction side at the design point operating under the straight shaft and inclined shaft conditions are demonstrated in **Figure 12**. It is indicated that the shape of pressure distribution (pressure side and suction side) on each blade of the propellers is identical when operating under the straight shaft condition, because there is no unstable force due to the cross-flow with the inclined shaft condition. Meanwhile, the pressure distribution contours (pressure and suction sides) on each blade of propellers operating under the inclined shaft angle are different because each blade generates an unbalanced load. The average pressure distribution on the pressure side of the blade's downward position is higher than the blade's upward position. On the contrary, the shape of the average pressure distribution on the suction side of the blade's downward position is lower than the blade's upward position. Therefore, this phenomenon may mainly cause cavitation and vibration, which is detrimental to the propeller.

Figure 13 shows the shape of the average pressure coefficient distribution on a long-drive shaft at the design point operating under the straight shaft and inclined shaft conditions. It is found that the fluctuations of the high fluid pressure occur around a long-shaft drive before entry of the propeller when operating under inclined shaft condition. Conversely, this is not observed for straight shaft conditions. This result confidently shows that unsteady flows with cross-flow occur around the entrance areas of the propeller. As a result, each blade creates unbalanced forces.

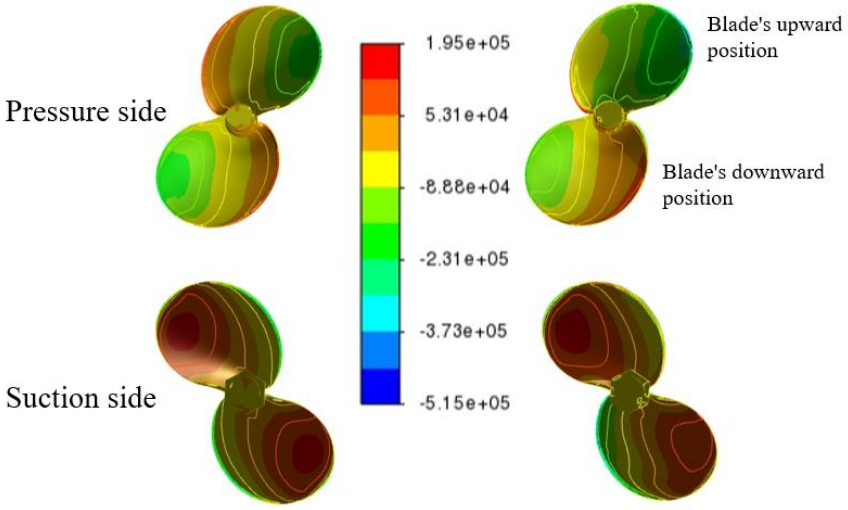

Figure 12 Shapes of pressure coefficient on pressure and suction sides with a long-drive shaft at the design point operating under the straight shaft condition (left) and the inclined shaft condition (right).

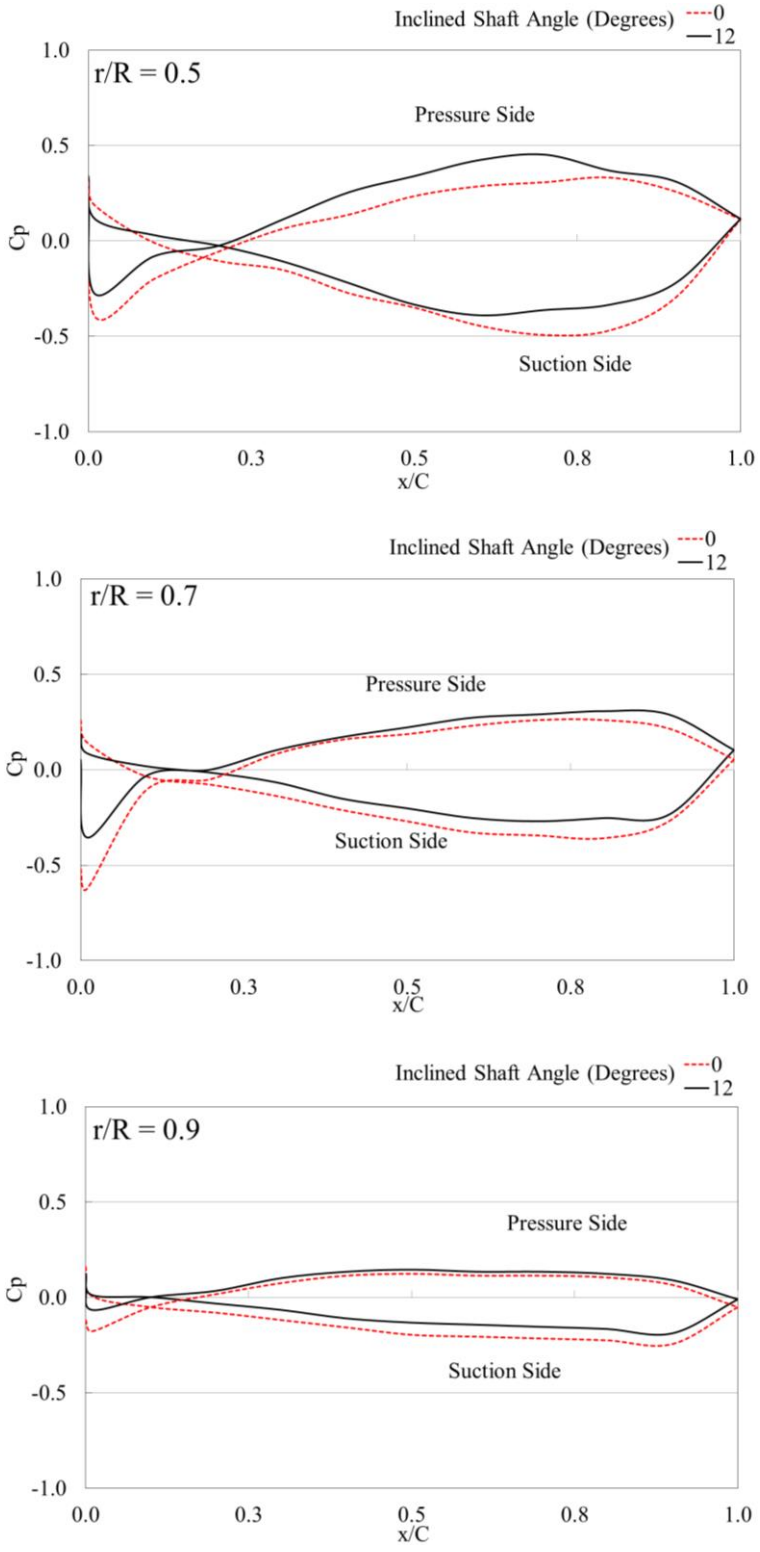

Figure 11 Pressure coefficients, chord-wise, of blade positions r/R = 0.5, 0.7, and 0.9 with a long-drive shaft at design point operating under the straight shaft and inclined shaft conditions.

The wake field around a long-drive shaft and propeller is described through velocity magnitude contours. The axial velocity fields in upstream of the propeller, with the cutting plane crossing the propeller center at x/R = 0.00, 0.25, 0.5, 0.75, and 1.0 at the design point operating under

the straight shaft and inclined shaft conditions, are illustrated in **Figure 14**. It is found the average velocity contours at the center of the propeller plane (x/R = 0.00) and at the adjacent propeller center plan (x/R = 0.25) showed similarity around each propeller blade when operating under straight shaft conditions. This is to confirm that a long-drive shaft does not affect the fluid flow at the propeller entrance when operating under the straight shaft conditions. Meanwhile, for the velocity contours at x/R = 0.00 and 0.25, the area around the blade's downward position is lower than the area around the blade's upward position when operating under the inclined shaft angle. It is affected by a long-drive shaft that interferes with the fluid flow at the propeller entrance. Therefore, this is one of the reasons why the blade generates forces with non-equilibrium. However, the average velocity shapes at the center of the propeller plane (x/R > 0.50) are similar around the area of the blade's downward position and the blade's upward position for both cases.

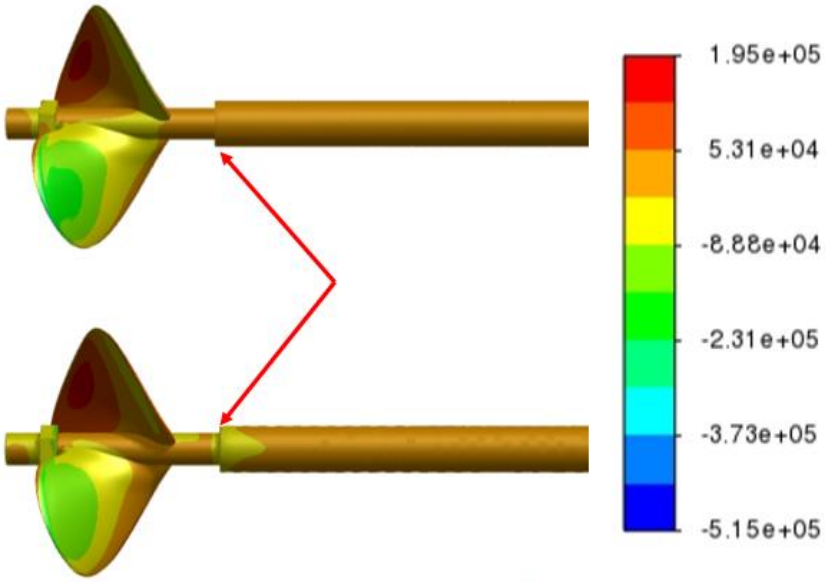

Figure 13 Pressure coefficient contours on a long-drive shaft at the design point operating under the straight shaft condition (upper) and the inclined shaft condition (lower).

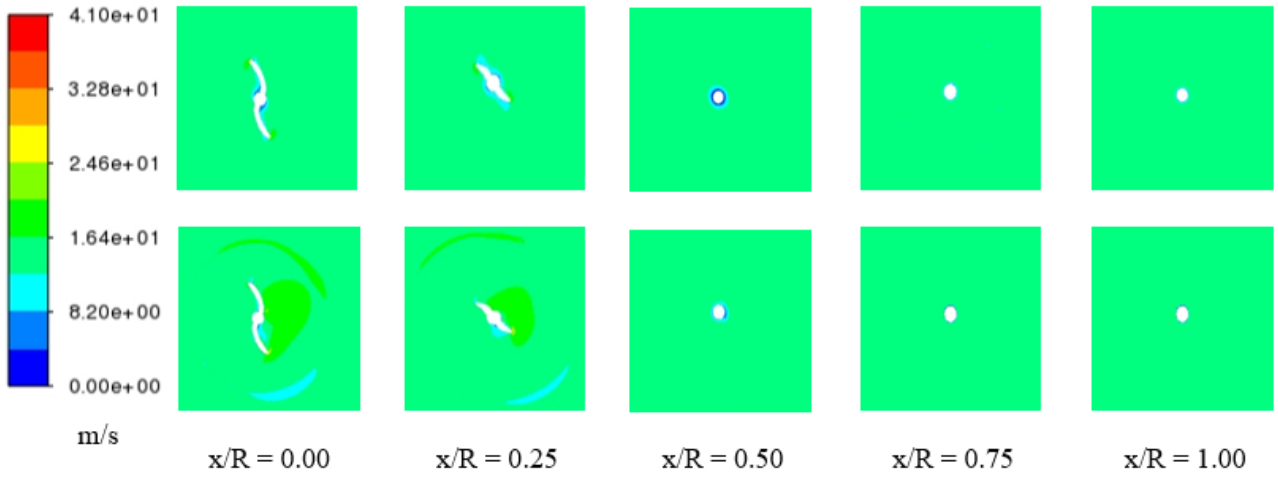

Figure 14 Shapes of velocity magnitude upstream of the propeller at x/R = 0.00, 0.25, 0.5, 0.75, and 1.0, respectively, at the design point operating under the straight shaft condition (upper) and operating under inclined shaft angles (lower).

Figure 15 demonstrates the axial velocity fields in downstream of the propeller with the cutting plane crossing the propeller center at x/R = 0.00, 0.25, 0.5, 0.75, 1.0, 1.5, and 2.0 at the design point operating the straight shaft and inclined shaft conditions. The average velocity contours at the center of the propeller plane at each range of position have seemed similar between around the blade's downward position and the blade's upward position for operating straight condition. It ensures that a long-drive shaft does not influence the unbalanced load of the propeller operating straight condition. Contrary, the velocity contours at the center of the propeller plane at each range of position showed the difference between the blade's downward position and the blade's upward position with operating the inclined shaft angles. It is believed to create an unsteady force by the propeller.

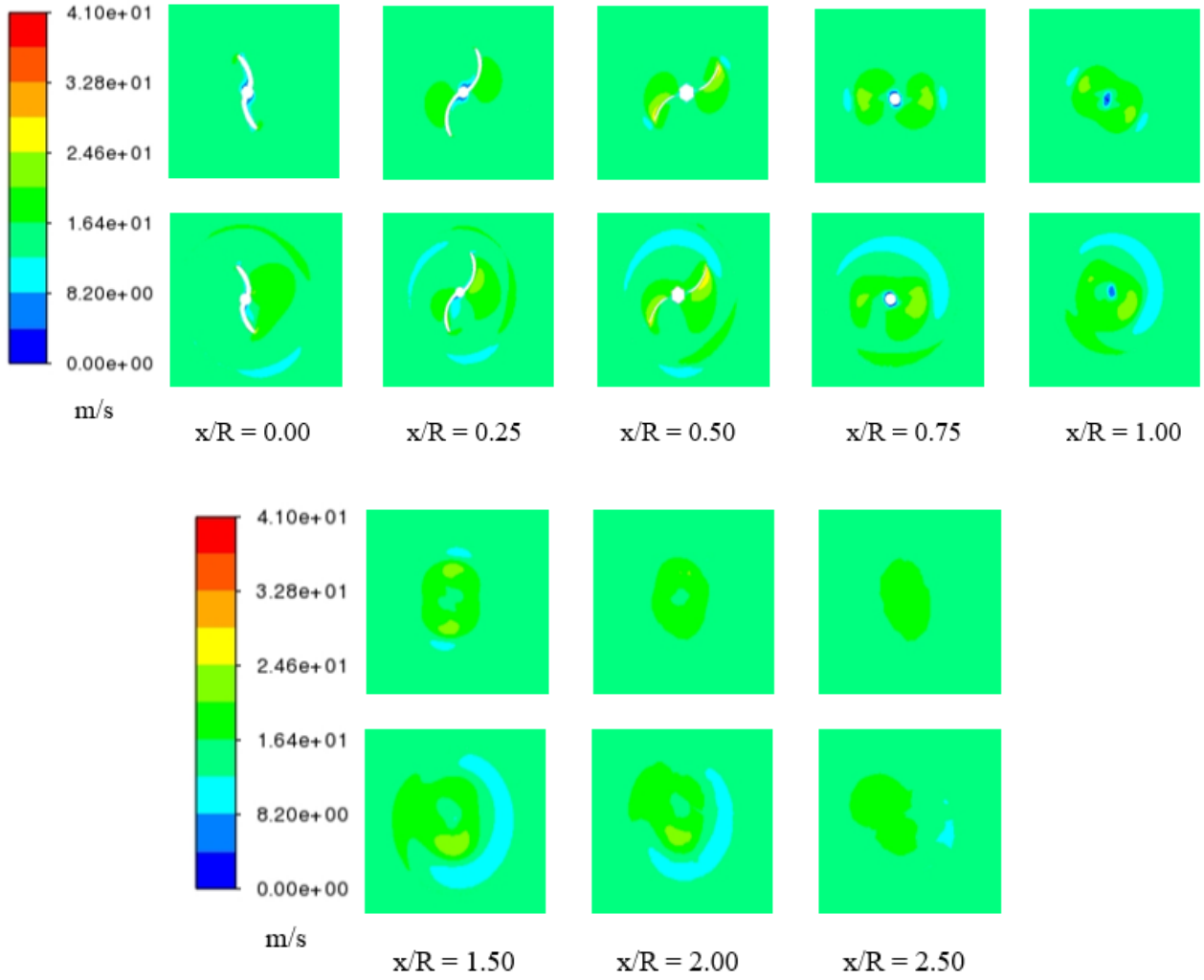

Figure 15 Shapes of velocity magnitude downstream of the propeller at x/R = 0.00, 0.25, 0.5, 0.75, 1.00, 1.50, 2.00, and 2.50, respectively, at the design point operating under the straight shaft condition (upper) and operating under inclined shaft angles (lower).

6. Conclusions

CFD results of the thrust, torque coefficients, and propeller efficiency operating without an inclined shaft angle have been compared to measurement data in open water tests for the model-scale propeller size. The numerical and experiment results are in very good agreement at each range of advance coefficients [J], as well as at the design point. Moreover, the calculation results without a long-drive shaft for the full-scale propeller size agree well with the experimental data.

The computational results of unsteady propeller performance when operating under the straight shaft conditions show that the values with a long-drive shaft are lower than those without a long-drive shaft at each range of advance coefficient [J]. At the design point, the total thrust, torque, and propeller efficiency with a long-drive shaft are reduced by approximately 3.14, 1.96, and 1.2 %, respectively, compared to those without a long-drive shaft. These results are because the long-drive shaft blocks the fluid flow entering the propeller. Thus, it generates drag forces on the vessel.

The propeller efficiency with a long-drive shaft for an inclined shaft angle corresponding to the Long-Tail Boat in sea trials in a river in Thailand are decreased compared to those for operating under straight shaft conditions at each range of advance coefficient [J]. The propeller efficiency with a long-drive shaft for an inclined shaft angle compared to the straight shaft conditions decreased by about 3.21 % at the design point. It is also found that the propeller efficiency is significantly reduced when the advance coefficient or flow velocity is high. The reason for this is that the fluid flow phenomenon around the propeller blade is complicated for the inclined shaft angles. The velocity of flow between the blade's upward position and the blade's downward position is different. Thus, the thrust and torque are created unevenly, according to each angle of propeller rotation. Furthermore, one reason for these results is because the propeller characteristics, in terms of pitch distribution, skew, and rake angles, have been not designed for operating under inclined shaft angles. Therefore, the propeller generates unstable thrust and torque, which causes decrease in the propeller efficiency.

The long-drive shaft operating under the straight shaft condition has no drag forces in each range of advance coefficient. However, it is influential when operating under inclined shaft angles where drag forces are proportional to the advance coefficient [J] or inflow velocity. The pressure coefficient distributions at each radius of the blade operating under the inclined shaft angles are more aggressive than operating under the straight shaft condition, which correspond to the pressure distributions on the suction and pressure sides. The upstream and downstream velocity fields at each position from the distance of the propeller center for operating under the inclined shaft angles are shown to be more irregular than for operating under the straight shaft conditions.

The results of this research indicate that a long-drive shaft creates drag force, which affects the total thrust, especially when defined as the inclined shaft condition. Therefore, the long-drive shaft should be designed in suitable for operating the inclined shaft conditions because it will directly affect the propeller efficiency. Such as the shape, size, and length of the shaft should be considered when designing a long-drive shaft. It can be said that CFD is an invaluable tool for researchers, it makes to understand the behavior of complex fluids. This can help design and modify the long-drive shaft to be suitable.

References

Abbasi, A.A., Franzosi, G., Canepa, E., Gaggero, S., Villa, D., Viviani, M., & Tani, G. (2023). Experimental analysis of the flow field around a propeller with inclined shaft. *Ocean Engineering*, 285, 115-237. https://doi.org/10.1016/j.oceaneng.2023.115237

Aktas, B., Atlar, M., Turkmen, S., Korkut, E., & Fitzsimmons, P. (2015). Systematic cavitation tunnel tests of a Propeller in uniform and inclined flow conditions as part of a round robin test campaign. *Ocean Engineering*, 120, 136-151. http://dx.doi.org/10.1016/j.oceaneng.2015.12.015

Alder, R. S., & Moore, D. H. (1977). *Performance of an inclined shaft partially-submerged propeller operating over a range of shaft yaw single*. David, W. (Ed.). Taylor Naval Ship Research and Development Center, Bethesda, Maryland, USA.

ANSYS Fluent Theory Guide. (2021). ANSYS.

ANSYS Fluent User's Guide. (2021). ANSYS.

Efremov, D. (2021). Determining the loss of efficiency of twin propeller systems in circulation maneuvers. *Maritime Technology and Research*, 3(2), 89-101. https://doi.org/10.33175/mtr.2021.244703

Gaggero, S., & Villa, D. (2018). Cavitating propeller performance in inclined shaft conditions with OpenFOAM: PPTC 2015 Test Case. *Journal of Marine Science and Application*, 17, 1-20. https://doi.org/10.1007/s11804-018-0008-6

Kaewkhiaw, P. (2018). *The effect of shaft yaw angles on propeller performance for Long-Tail Boat using CFD*. In Proceedings of the 13th International Conference on Hydrodynamics, Incheon, Korea.

Kaewkhiaw, P. (2020). CFD analysis of unsteady propeller performance operating at different inclined shaft angles for LONG-TAIL boat in Thailand. *Journal of Naval Architecture and Marine Engineering*, 17(2), 115-127. http://dx.doi.org/10.3329/jname.v17i2.42622

Kaewkhiaw, P. (2021). Numerical study of propeller boss cap fins on propeller performance for Thai Long-Tail Boat. *Ocean Systems Engineering, 11*(4), 373-392. https://doi.org/10.12989/ose.2021.11.4.373

Kaewkhiaw, P., Yoshitake, A., Kanemaru, T., & Ando, J. (2015). Experimental and numerical study of propeller performance for Long-Tail Boat in Thailand. *The Japan Society of Naval Architects and Ocean Engineers, 20*, 407-410.

Ortolani, F., & Dubbioso, G. (2019). Experimental investigation of single blade and propeller loads by free running model test. Straight ahead sailing. *Applied Ocean Research, 87*, 111-129. https://doi.org/10.1016/j.apor.2019.03.005

Ortolani, F., & Dubbioso, G. (2019). Experimental investigation of blade and propeller loads: Steady turning motion. *Applied Ocean Research*, 91, 101874. https://doi.org/10.1016/j.apor.2019.101874

Ortolani, F., Capone, A., Dubbioso, G., Pereira, F. A., Maiocchi, A., & Felice, F. D. (2020). Propeller performance on a model ship in straight and steady drift motions from single blade loads and flow field measurements. *Ocean Engineering, 197*, 106881. https://doi.org/10.1016/j.oceaneng.2019.106881

Paik, K. J., Jang, Y. H., Eom, M. J., Kim, S. H. & Song, G. (2020). A numerical study on the open water performance of a propeller with sinusoidal pitch motion. *Brodogradnja/Shipbuilding, 71*(1), 71-83. http://dx.doi.org/10.21278/brod71105

Peck, J. G., & Moore, D. H. (1974). *Inclined-shaft propeller performance characteristics.* Report of SNAME, New York, USA.

Practical Guidelines for Ship CFD Applications. (2011). *ITTC recommended procedures and guidelines*.

Seyyedi, S. M., Shafaghat, R., & Siavoshian, M. (2019). Experimental study of immersion ratio and shaft inclination angle in the performance of a surface-piercing propeller. *Mechanical Sciences, 10*, 153-167. https://doi.org/10.5194/ms-10-153-2019

Soares, C. G., Tadros, M., & Ventura, M. (2022). An optimization procedure for propeller selection for different shaft inclinations. *International Journal of Maritime Engineering, 164*(A3), A295-A315. https://doi.org/10.5750/ijme.v164iA3.809

Taniguchi, K., Tanibayashi, H., & Chiba, N. (1969). *Investigation into the propeller cavitation in oblique flow*. Mitsubishi Technical Bulletin, Japan.

Wang, C., Sun, S., Sun., S., & Li, L. (2017). Numerical analysis of propeller exciting force in oblique flow. *Journal of Marine Science and Technology*, *22*, 602-619. https://doi.org/10.1007/s00773-017-0431-4

Yao, J. (2015). Investigation on hydrodynamic performance of a marine propeller in oblique flow by RANS computations. *International Journal of Naval Architecture and Ocean Engineering*, *7*, 56-69. http://dx.doi.org/10.1515/ijnaoe-2015-0005

Zheng, C., Hong, F., Zhang, Z., & Liu, D. (2022). *The numerical investigation of propeller cavitation benchmark tests in oblique flow*. In Proceedings of the 7th International Symposium on Marine Propulsors, Wuxi, China.